SSCL-Preprint-551

SSCL-Preprint-551
January 1994
Distribution Category: 400

V. T. Kovachev
M. J. Neal
D. W. Capone II
W. J. Carr, Jr.
C. Swenson

Interstrand Resistance of SSC Magnets

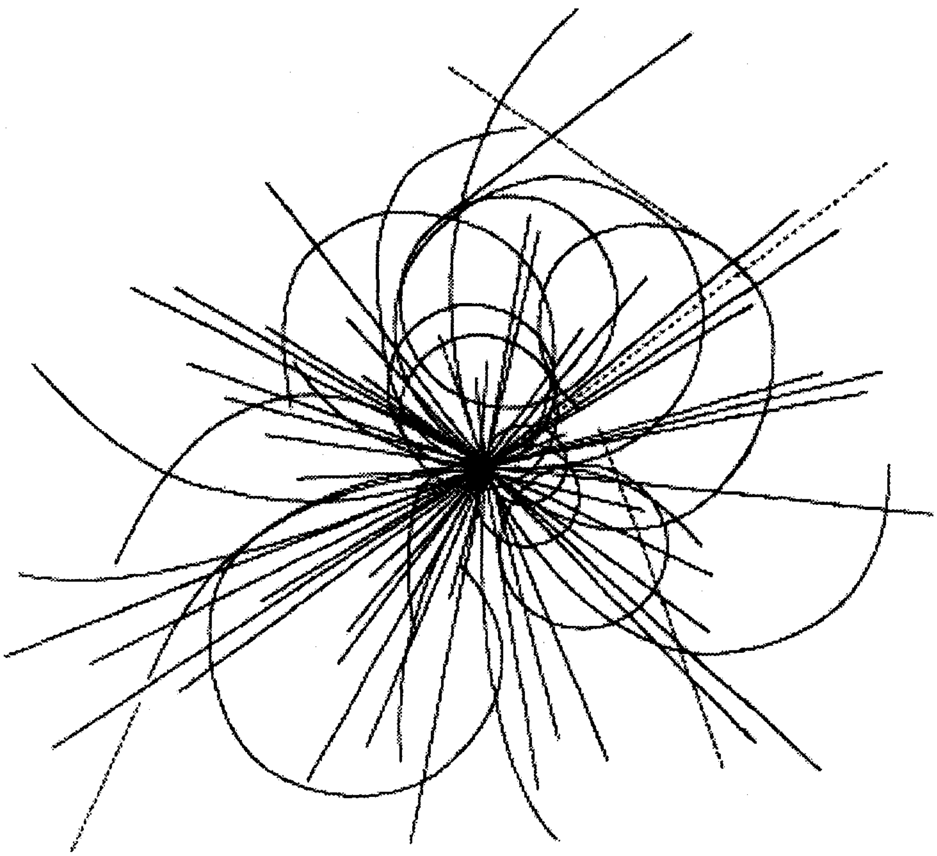

Superconducting Super Collider Laboratory

SSCL-Preprint-551

Interstrand Resistance of SSC Magnets*

V. T. Kovachev, M. J. Neal, and D. W. Capone II

Superconducting Super Collider Laboratory†
2550 Beckleymeade Ave.
Dallas, TX 75237

W. J. Carr, Jr. and C. Swenson

Westinghouse Electric Corporation
Science and Technology Center
1310 Beulah Rd.
Pittsburgh, PA 15235

January 1994

---

*To be submitted to the *Journal of Cryogenics*.

†Operated by the Universities Research Association, Inc., for the U.S. Department of Energy under Contract No. DE-AC35-89ER40486.

INTERSTRAND RESISTANCE OF SSC MAGNETS

V. T. Kovachev, M. J. Neal, and D. W. Capone II

Superconducting Super Collider Laboratory*
2550 Beckleymeade Ave. Dallas, TX 75237-3997

W. J. Carr, Jr. and C. Swenson

Westinghouse Electric Corporation
Science and Technology Center
1310 Beulah Rd.
Pittsburgh, PA 15235

ABSTRACT

In situ interstrand resistance measurements were conducted on selected section of the inner coil of a full size (15 m) and a short (1 m) model SSC magnets. A model for evaluating single contacts resistance between two strands was developed. Using this model analyses of adjacent and non-adjacent strand contacts were performed. The interstrand resistance distribution throughout the coil was found to correlate with the quench location data as well as with the multipoles decay characteristics of the magnet. An anisotropic continuum based model for evaluation of cable eddy current losses was developed and results were compared with the experimental data.

keywords: interstrand resistance, quench location, cable eddy current losses.

---

*Operated by the Universities Research Association, Inc., for the U.S. Department of Energy under Contract No. DE-AC35-76SF00098.

I. INTRODUCTION

The performance of full length SSC dipole magnets has demonstrated that 50 mm aperture dipoles were much more sensitive to the current ramp rate than their predecessors with 40 mm aperture.[1] Moreover, the magnet quench current (Iq) at high ramp rates exhibited a very large magnet-to-magnet spread. There were two quite distinct families of curves for the quench current vs. the current (field) ramp rate of full length dipole magnets. The first one (type A) showed an initially nearly flat quench current up to about 20 A/s, then an almost linear decrease of the quench current with the ramp rate. The linear portion of the Iq(dI/dt) curve, however, varies significantly among the magnets of this family. The second family of magnets (type B) showed a rapid initial decrease in quench current at low ramp rates followed by an almost constant quench current at high ramp rates. The 50 mm SSC short model dipoles basically have shown similar behavior but somewhat less pronounced.

Energy loss during the field ramp of type A and type B magnets were also different. Type A magnets exhibited very large eddy current losses at high ramp rates. Type B dipoles had a relatively small eddy current loss during the ramp. It was suggested that the eddy current dissipation due to interstrand currents was playing a critical role in the magnet behavior and that the interstrand resistance was varying considerably among magnets resulting in differences observed in the total amount of eddy current loss. There was indirect experimental evidence that quenches in magnets were related to this extra eddy current energy release. When such a magnet was excited slowly (for instance with a ramp rate of about 10 A/s) the quench locations were at the magnet pole because the field intensity at the pole site of the inner coil is the highest. When the ramp rate was increased, the quench current went down and the quench location moved to the multi-turn section of the inner coil where the magnetic field has a larger angle with the wide face of the cable and large interstrand eddy currents results. This is also the region of the coil where heat removal is most difficult. Large eddy current loss and quench location shifting to the multi-turn section suggested an existence of relatively low interstrand resistance in the bulk of the magnet inner coil.

The aim of the present work was to obtain accurate data for interstrand resistance and interstrand resistance distribution in SSC magnets and to find a correlation between the interstrand resistance and the magnet performance. For this purpose a novel *in situ* technique was used for interstrand resistance measurements, a simple model for evaluation of individual interstrand contacts was applied, and a new approach for calculation of interstrand eddy current losses was developed.

II. EXPERIMENTAL

II.1 Magnets under study

The quench current ramp rate sensitivity of the full length SSC dipole DCA312 was strongly A-type and the eddy current losses for this magnet (approximately 65 J/A/s for a standard monopolar cycle) were the largest of all SSC magnets built.[1] In order to find the cause of the anomalous behavior of DCA312, it was decided that the magnet would be cut into sections and examined. The general goals of the DCA312 autopsy included verification of theoretical models for SSC magnets behavior as well as correlation of magnet fabrication and assembly procedures to the quench behavior.[2] One of the important aspects of the magnet autopsy plan was the *in-situ* measurement of interstrand resistance in collared magnet sections. Four sections of DCA312 were designated for interstrand resistance measurements. Two of those sections (C and M) contained quench sites (for 100 A/s and 200 A/s ramp rates respectively) and two of them (E and J) were sections representative of the magnet where quenches did not occur. According to the quench test data for DCA312 the 100 A/s quenches occurred in the inner coil 6.95 m from the centerline toward the non lead end of the magnet and azimuthally between 141° and 177° counterclockwise from the right hand horizontal axis as viewed from the lead end of the magnet. This region incorporates turns 2 through 11 of quadrant 1 as viewed from the magnet non-lead end. The 200 A/s quenches occurred in the inner coil 4.17 m from the centerline toward the non-lead end of the magnet and azimuthally between 22° and 36° counterclockwise from the right hand horizontal axis as viewed from the lead end of the magnet. This region incorporates turns from 7 through 11 of quadrant 3 as viewed from the magnet non-lead end.

The quench current behavior of the short SSC model magnet DSA328 was approximately B type - almost a flat quench current up to about 50 A/s and type B-like decrease (but more rapid than usual) of the quench current with the ramp rate up to 300 A/s. The first quenches (at $dI/dt < 20$ A/s) have occurred at the inner pole turn splice side. At $dI/dt > 20$ A/s the quenches have moved to the multiturn section of the inner coil. The AC losses measurements for magnet DSA328 have shown relatively small eddy current loss of 0.62 J/(A/s) per monopolar cycle.

II.2 Preparation of magnet sections

Four sections of the magnet DCA312 and one section of DSA328 were prepared for *in situ* interstrand resistance measurements .[3,4] The yokes of these sections were removed but the collars were left on the tested region of each section. All four keys were spot-welded every 2-3 cm in a zig-zag manner on both key sides of the collar to insure that collar pressure was maintained. The collared portion was approximately one cable twist pitch (88 mm ±5%) in length. The collar and outer coil were removed from one end of the sections from an approximately 45-65 mm length for purposes of making electrical connection to the strands of inner coil. Each section was polished at the collared end using an Automet polisher set on 150

RPM. The following grits of silicon carbide sandpaper were used for a duration of 5 minutes each: 120, 180, 240, 320, 400 and 600. The sample was washed with water between each grit to reduce carry over. Each section was then etched with a solution of 20 % Nitric acid in water for 15 - 20 seconds. The section was then rinsed with water and inspected with a 10X microscope to make sure there was no smearing of copper between the strands which might result in erroneous resistance readings when tested. Following the interstrand resistance measurements the magnet sections were disassembled and each turn was examined under an optical microscope.

II.3 Test procedure

The *in situ* interstrand resistance measurements were performed using the standard four-probe technique. The current leads were made of teflon insulated 10 gauge copper wire. The bottom portion of the current leads consists of 15-20 cm of NbTi multifilamentary wire (SSC inner strand) to allow easy connection to the test section and to reduce the heat to the LHe bath. The voltage taps were made of varnish insulated 30 gauge copper wire. Two sample holders have been built. Each of the sample holders consist simply of two flanges made of G-10 fiberglass (250 mm and 140 mm in diameter) and a G-10 rod (16 mm in diameter) connecting these two flanges. The coil section is situated on the 140 mm flange and instrumented with current and voltage tap leads. The upper flange serves as a top plate for the cryostat. Prior to cooling down to 4.2 K the magnet section was precooled to LN temperature then inserted into the helium cryostat. A simple LHe dewar with superinsulation and large aperture was used as the 4.2 K cryostat. The turns of the inner coils were labeled in the conventional manner from 1 (midplane turn) to 19 (pole turn).

In one cool down the inner coil turns were tested for interstrand resistance in pairs, one turn from each of the two coils (from quadrants I and III, and II and IV respectively). As each measurement of one turn in a coil was completed the strand ends of that turn were cut away to reveal the strand ends of the next turn. The cable strands at a given test point were labeled from 1 to 30 counterclockwise from the inside minor edge of the cable as shown in Figure 1. In this way, starting from the pole toward the midplane the turns of both coils in the magnet were measured in succession. The measurements were carried out at 4.2 K. A sample current of 10-50 Amps (typically 30 A) was used and a voltage drop of 1-100 μV across the two strands was recorded. Voltage averages were reproducible to within 5%, irrespective of thermal cycling and reinstrumentation of current and voltage leads. The typical thermal voltage was not greater than 1 μV. The current was supplied by a Hewlett Packard 6031A System Power Supply and the voltage was recorded using a Keithley 182 Sensitive Digital Voltmeter. Output from the power supply was passed through a zero flux transformer, inducing a proportional voltage in the transformer which was monitored by another Keithley 182 Voltmeter. The voltage used in resistance calculations was the average of 200 consecutive readings taken at 25 ms intervals using the data storage function of the Keithley 182 Sensitive Digital Voltmeter. The experimentally obtained values for interstrand resistances were calculated from the average voltage using a Microsoft Excel 4.0 spreadsheet package.

For the DSA328 section all 19 turns of quadrants II and IV were measured in succession. A set of six strands consisting of equally spaced non-adjacent strands (1, 6, 11, 16, 21, and 26, see Figure 1) was tested for each turn of both quadrants. In addition, a set of six adjacent strands (1-6) was tested for turns 16-19 of both quadrants and turn 1 of the upper coil. The six strands in each set were paired for testing in all possible combinations, generating a total of 15 resistance measurements for each cable. The entire set of data for the interstrand resistance of the DSA328 inner coil contains approximately 750 interstrand resistance values.[4]

For DCA312 sections the set of strands within a turn and the set of turns within a section chosen for testing were modified. Typically a set of 9 turns from each quadrant was tested. These nine turns were: 1, 3, 6, 7, 13, 14, 16, 17, and 19. In addition all turns in the regions identified as quench locations were tested. The quench locations were: section C, quadrant I, turns 2-11 (100 A/s quench) and section M, quadrant II, turns 7-10 (200 A/s quench). Eight of the thirty strands in a cable turn were instrumented for interstrand resistance testing. This set of strands was chosen to include the six strand set used in DSA328 measurements and to increase the variety of strand separations tested with a minimal increase in the number of measurements.

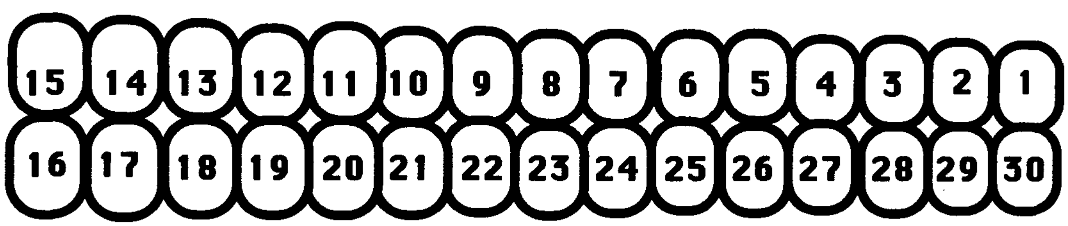

Figure 1 Sketch of 30 strand Rutherford cable cross section showing labeling scheme for *in situ* interstrand resistance measurements.

These strands were tested in all possible pairings resulting in a total of 28 interstrand resistance measurements from each turn. In addition to the standard sample set all thirty strands of one turn (Section E, quadrant III, turn 19) were tested. For this turn a total of 112 interstrand resistances were measured, including resistance between all adjacent strands. This more complete sampling of turn 19, (Section E, quadrant III) was performed to establish the validity of the standard sample set .

The entire set of data for the interstrand resistance of sections C, E, J, and M of DCA312 inner coil consists of approximately 8700 resistance values, each one calculated from the average voltage described earlier using a Microsoft Excel 4.0 spreadsheet package.[3]

III. RESULTS AND DISCUSSION

III.1 Adjacent and non-adjacent strand resistances

The obtained data for both DSA328 and DCA312 have shown that adjacent strand resistance is considerably lower than the resistance between non-adjacent strands. As an illustration of this the average adjacent strand resistance and the average non-adjacent strand resistance for turns 19-15 of upper and lower coil of DSA328 are presented in Table 1. This fact, which has never been considered before for Rutherford type cables, is to be expected due to the different nature of adjacent and nonadjacent contacts. In addition to the relatively large surface

Table 1. Average interstrand resistance values for adjacent and non-adjacent strand pairs of DSA328.

Turn #	Upper Coil		Lower Coil	
	Non-Adjacent μΩ	Adjacent μΩ	Non-Adjacent μΩ	Adjacent μΩ
19	11.7	3.0	5.0	3.0
18	5.8	1.4	3.3	1.3
17	0.8	0.2	2.4	1.1
16	1.9	0.3	3.2	1.8
15	1	0.2	1.5	0.4

area of adjacent strand side-by-side contact, the strands transpose at the edge of the cable so that they rollover one another. This rollover takes place over quite a long distance along the cable axis and involves more strand deformation than non-adjacent strand crossover. At the cable edges the compaction of the cable is largest. The experimental technique used for interstrand resistance measurements can not distinguish between side-by-side and rollover contacts. In reality a combination of both can cause low interstrand resistance between adjacent strands. It has also been found that the measured resistances between the adjacent strands and in particular between non-adjacent strands vary and in many cases are far from identical.

The measured interstrand resistance as a function of strand separation for a given turn of the magnet generally shows a second order polynomial type of curve, in some cases appearing as a simple parabola. Figure 2 shows data from turn 16 of the upper coil of DSA328 which has this parabolic shape and turn 19 of the lower coil of DSA328 which has the more general second order polynomial shape. As will be discussed below, in both cases predominate conductance

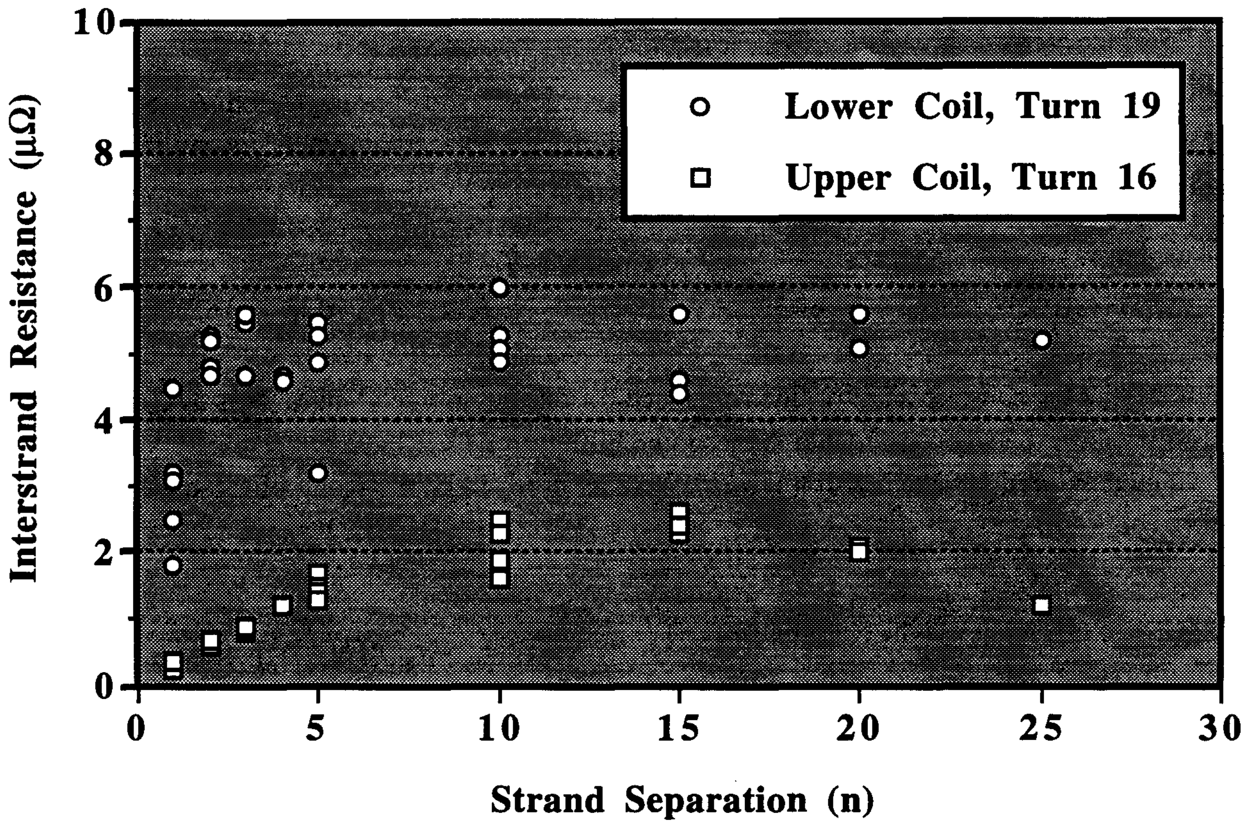

Figure 2 Interstrand resistance as a function of strand separation for turn 16 of the upper coil and turn 19 of the lower coil of DSA328.

between all strands must be identical otherwise the experimental data will not lie on the typical curves. The interplay between adjacent strand major contacts (rollover and/or side by side) and non-adjacent strands major contacts (crossover) will be explained below by means of a simple model.

III.2 Model for evaluation of single contact resistance

The model for the evaluation of single contact resistance between any two strands considers two limiting cases. In the first case rollover/side-by-side contacts are neglected. All crossover contacts are assumed equal to r_{co}. Each strand pair makes 2 crossover contacts in one cable pitch length. The two contacts are in parallel so that the primary resistance is $r_{co}/2$. In addition to this primary resistance the model considers secondary resistances in which an intermediate strand participates. Each secondary resistance is r_{co}, the sum of two primary resistances. All crossover paths beyond the secondary ones are neglected. For a cable with N strands there are N-2 secondary resistances and one primary resistance all acting in parallel so that a single measured crossover resistance is given by:

$$R_{co} = {r_{co}}/{N} \quad (1)$$

In the second case the crossover contacts between strands are neglected. In this case the circuit consists of two parallel sets of serially connected adjacent contacts. A single measured rollover/side by side resistance is given by:

$$R_{tot} = {r_{co} r_{adj} n(N-n)}/{N(r_{co} + r_{adj} n(N-n))} \quad (2)$$

where r_{adj} is the rollover/side by side resistance for one cable pitch length, N is as before, and n is the difference between strand numbers shown in Figure 1.

The measured resistances in this work were assumed to be the result of these two networks in parallel:

$$R_{tot} = {r_{co} r_{adj} n(N-n)}/{N(r_{co} + r_{adj} n(N-n))} \quad (3)$$

where r_{co}, r_{adj} , N, and n are as above. A more complete model, which considers the effect of paths which include both crossover and adjacent contacts yielded values for adjacent contact resistance in general agreement with those based on this simple model and crossover contact resistances which are up to 30% larger.[5] For purposes of the analysis presented in this paper, this level of agreement is acceptable and results from the simple model are used. Equation 3 can be manipulated algebraically to form Equation 4, which is a linear equation in 1/R and (N/(Nn-n^2)).

$$\frac{1}{R_{tot}} = \frac{1}{r_{adj}}\left({N}/{(Nn - n^2)} \right) + \frac{N}{r_{co}} \quad (4)$$

It is clear from Equation 4 that a plot of measured interstrand conductance (1/R) as a function of the strand separation parameter (N/(Nn-n^2) will be a straight line, the slope of which is the adjacent (side-by-side/rollover) interstrand conductance, and the y-axis intercept the product of N and the nonadjacent (crossover) interstrand conductance. Central to this analysis are the assumptions that all side-by-side/rollover resistances and all crossover resistances are identical. The extent to which this assumption is not valid will be reflected in the deviation of the data from linearity.

Figure 3 shows interstrand resistance data from turns 1 and 15 of the DSA328 upper coil plotted in the coordinate system of Equation 4. Adjacent strand data is plotted at the extreme right in this graph, and the apparent spread in this data is due to the low resistance values measured and the fact that the data is plotted as a conductance. For example, in the data presented for turn 15, n=1 ranges only from 0.18 to 0.26 μΩ, and for n=15 the range is from 1.2 to 1.3 μΩ. The data from these two turns are representative of the range of behaviors observed throughout the DSA328 magnet section. As can be seen from Figure 3, the adjacent strand resistance is typically at least an order of magnitude less than the crossover resistance and these values themselves can vary over an order of magnitude. The spread in the data at a given point along the x-axis can exceed the measurement error, indicating that individual resistances within the crossover and adjacent strand networks are not identical.

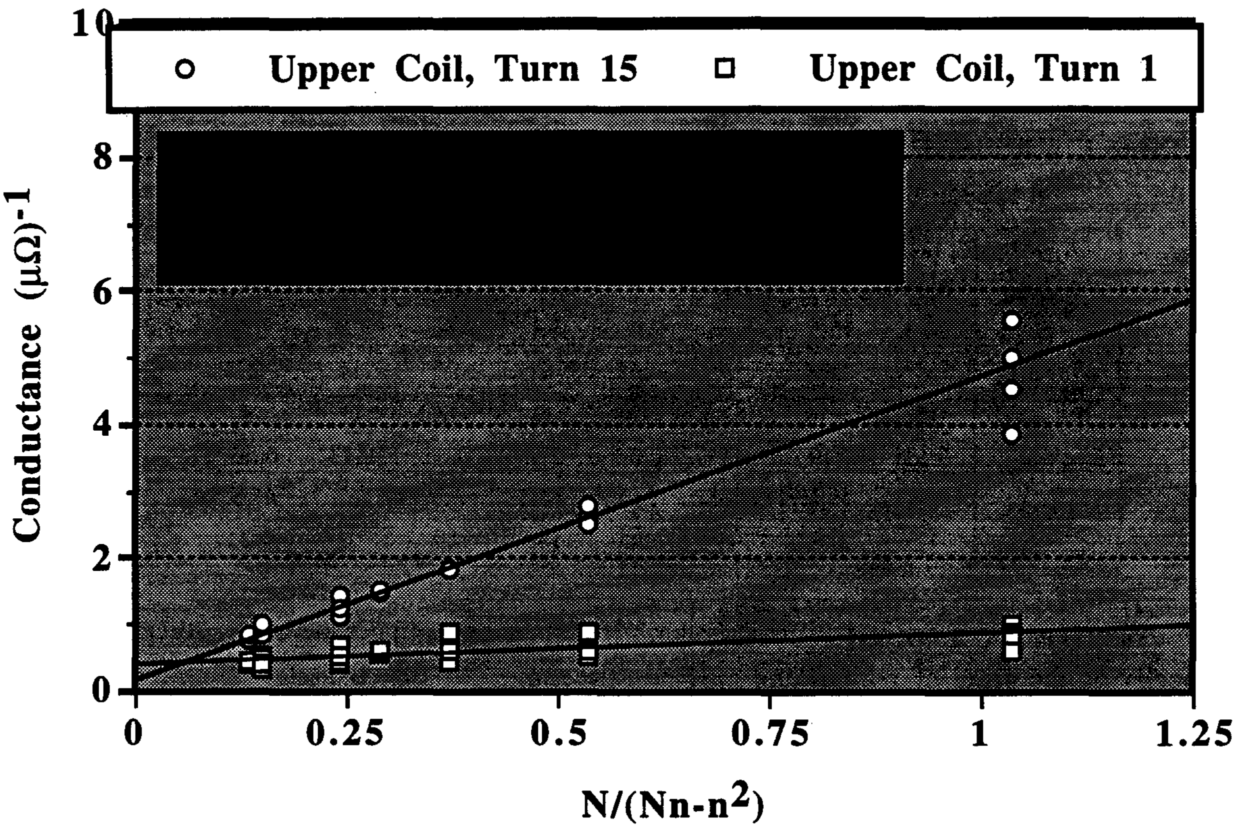

Figure 3. Measured interstrand conductance of DSA328 as a function of the strand separation parameter $N/(Nn-n^2)$ for two different turns of the upper coil. The straight lines are linear fits to the data and the values reported for r_{co} and r_{adj} are taken from these linear fits.

The evaluation of single crossover and adjacent contact resistances was carried out by the Excel 4.0 spreadsheet program using the analytical model previously described.

III.3 DCA312 quench regions

Figure 4 shows measured adjacent interstrand resistance and average measured interstrand resistance as a function of turn number for section C, QI of DCA312 and is representative of a quench site portion of the magnet inner coil. The average measured resistance was obtained by taking the average of all interstrand resistances measured regardless of the strand separation number. One can see that throughout most of the quench region (turn #2 through turn #11) both the adjacent and the average measured resistances are as low as 30-50 nΩ. A special feature of the quench region is that the average measured resistance is rather close to the measured adjacent resistance which suggests that the cable there has reduced anisotropy of effective resistivity[6] and that the effective resistivity, in general, is very low. Similar behavior of the measured interstrand resistances can be seen at the 200 A/s quench site, which supports the conclusion made above that, in these regions, the cable is like a solid bar of a nearly isotropic metal.

Table 2 presents calculated individual adjacent (r_{adj}) and crossover (r_{co})resistances vs. turn number for section C, QI. Adjacent resistances are evaluated per one cable pitch length and

Table 2. Calculated adjacent (r_{adj}) and crossover (r_{co}) resistances, and ratio r_{co}/r_{adj} for quadrant I, Section C, magnet DCA312 for several turns in the inner coil.

Turn #	1	2	3	4	4	6	7	8	9
r_{adj} (μΩ)	0.70	0.31	0.08	0.11	0.66	0.08	0.17	0.60	0.21
r_{co} (μΩ	24.4	15.5	2.6	1.2	1.1	7.2	1.8	1.3	1.2
r_{co} / r_{adj}	35	50	33	11	2	90	11	2	6
Turn #	10	11	12	13	14	16	17	19	
r_{adj} (μΩ)	0.10	0.19	0.09	0.09	0.07	0.08	0.13	0.58	
r_{co} (μΩ)	1.7	43.4	89.2	320	12.8	3.9	6.7	47.8	
r_{co} / r_{adj}	17	228	991	3560	183	49	52	82	

crossover resistances are per point contact. It can be seen that r_{co} in the quench region is typically on the order of 1-2 μΩ and r_{adj} is in the range of 0.08 - 0.7 μΩ. The ratio r_{co}/r_{adj} at the quench site varies from about 2 to 90 but in the middle of the quench site remains approximately equal to or less than 10 with the exception of the turn near the wedge (turn #6). The analytical model used to evaluate r_{co} is in principal much more accurate at values less than about 100 μΩ than at higher levels. This is because large crossover resistances result from ordinate intercepts very near zero in the linear fit method described above (see Figure 3). These

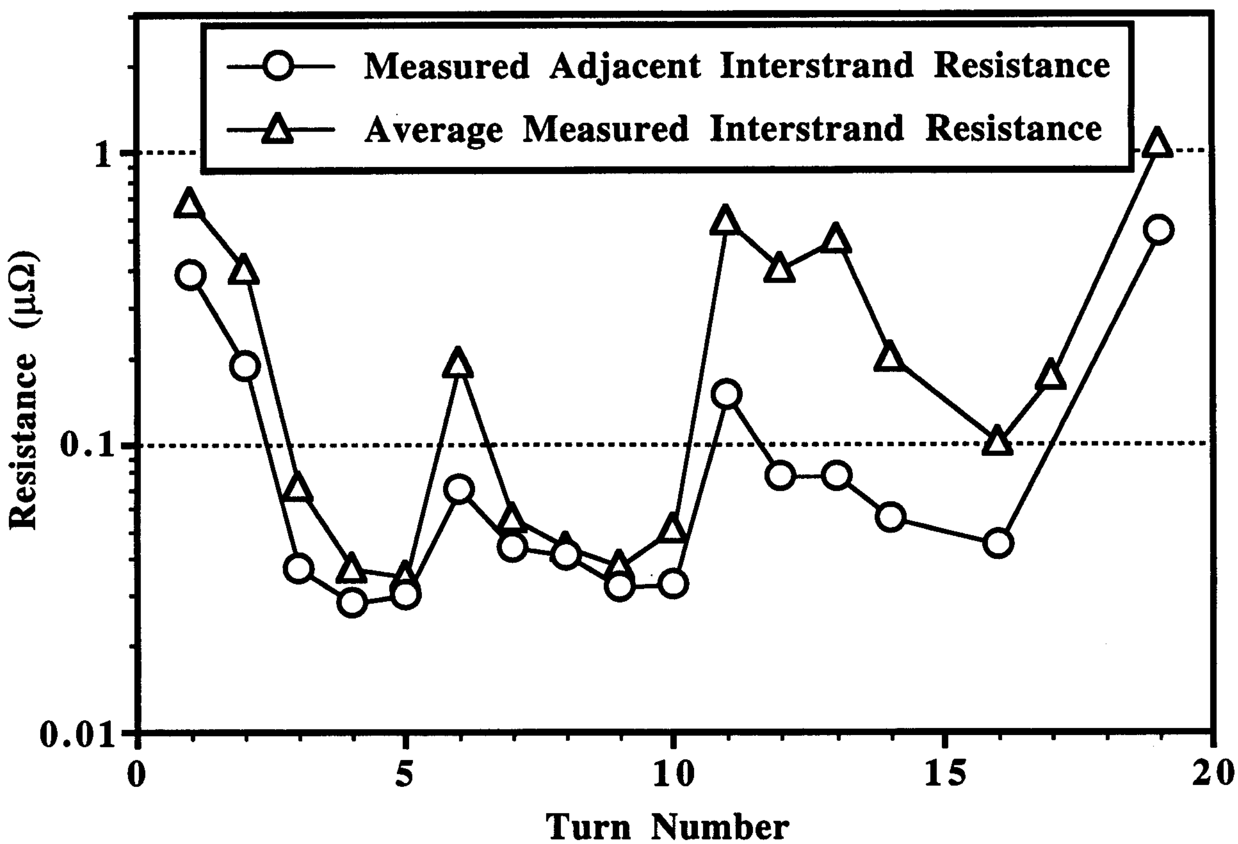

Figure 4. Measured interstrand resistance in section C , quadrant I of magnet DCA312, measured at each cable turn from the midplane (1) to pole (19) turns.

intercepts are the product of the crossover conductance and the number of strands so that small changes in the intercept near zero result in large variations in crossover resistances.

III.4 DCA312 non-quench regions

Figure 5 shows the measured adjacent and the average measured interstrand resistance for section J, QII of DCA 312 in which quenches have never occurred. Typically the interstrand resistance of non-quench sites is higher than at quench sites. As shown on Figure 5, in section J, QII the adjacent resistance is about 0.1 μΩ and most of the average measured crossover resistances are in the range of 0.3 - 0.7 μΩ. In some turns of non-quench sites the resistance is quite low and there is a rather close match between the adjacent and crossover resistances. However, in most of those cases either the neighboring turns have both adjacent and crossover resistances that are relatively large or the adjacent and crossover resistances are different. The latter can not be taken as a well established fact because not all of the neighboring turns have been measured.

Table 3 presents calculated individual adjacent (r_{adj}) and crossover (r_{co}) resistances vs. turn number for section J, QII. It can be seen that r_{co} of a non-quench section is primarily in the range of 10-100 $\mu\Omega$ and r_{adj} is in the range of 0.1-0.5 $\mu\Omega$. The ratio r_{co}/r_{adj} at the non-quench sites varies from about 7 to 450 but generally remains higher than 100.

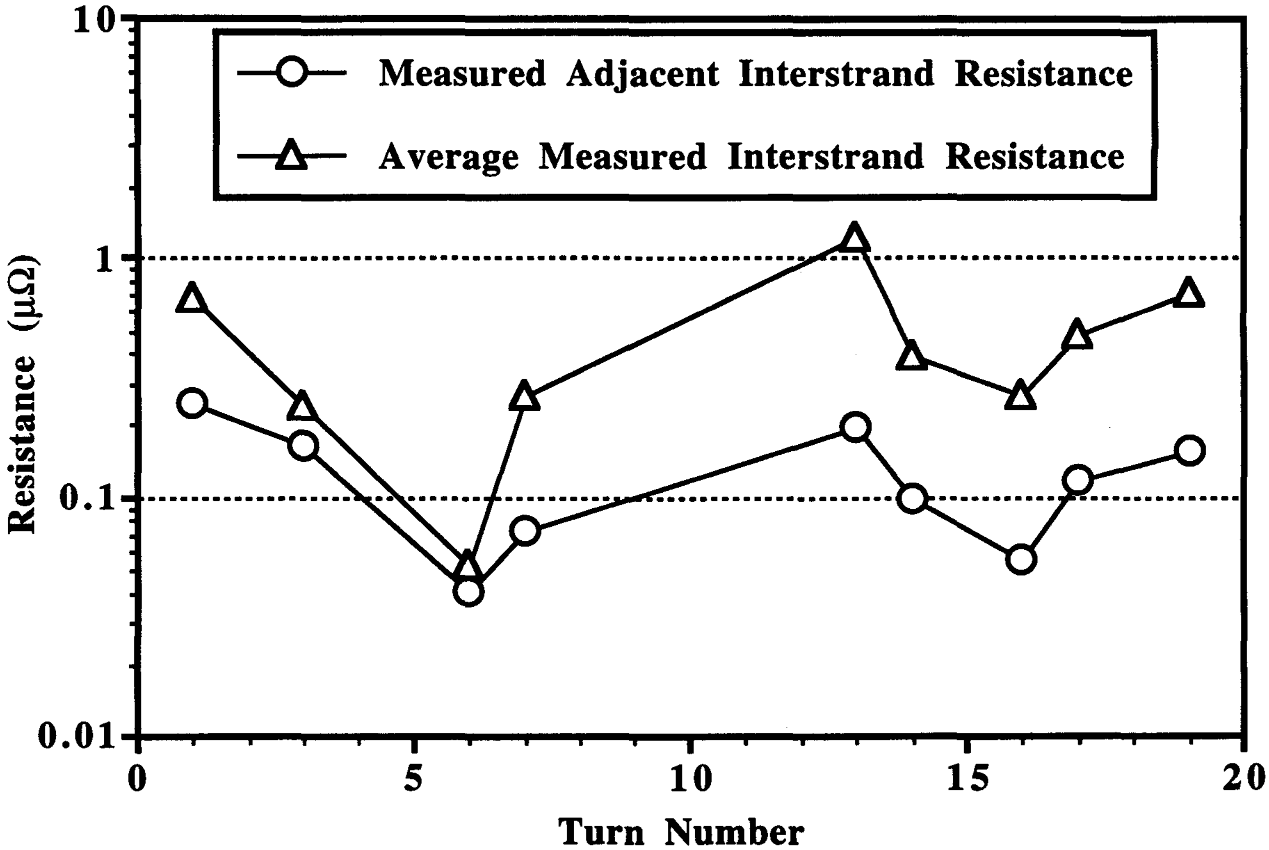

Figure 5 . Measured interstrand resistance in a non-ramp rate sensitive region (section J, QII) of magnet DCA312 plotted as a function of turn number.

Table 3. Calculated adjacent (r_{adj}), crossover (r_{co}) resistances, and ratio r_{co} / r_{adj} for quadrant II, Section J, magnet DCA312 for selected turns in the inner coil.

Turn #	1	3	6	7	13	14	16	17	19
r_{adj} ($\mu\Omega$)	0.34	0.50	0.24	0.09	0.24	0.12	0.07	0.14	0.19
r_{co} ($\mu\Omega$)	35.4	6.8	1.6	20.3	64.0	32.9	20.7	41.8	85.6
r_{co} / r_{adj}	104	14	7	226	267	274	296	299	451

III.5 Distribution of average resistance

The data obtained for DSA328 show that the average interstrand resistance through both the upper and the lower coils of the magnet has a tendency to be smaller nearer the midplane.[4] This is more pronounced for the upper coil than for the lower coil. Away from the pole turns the average interstrand resistance values for the upper and lower coils are about the same. However

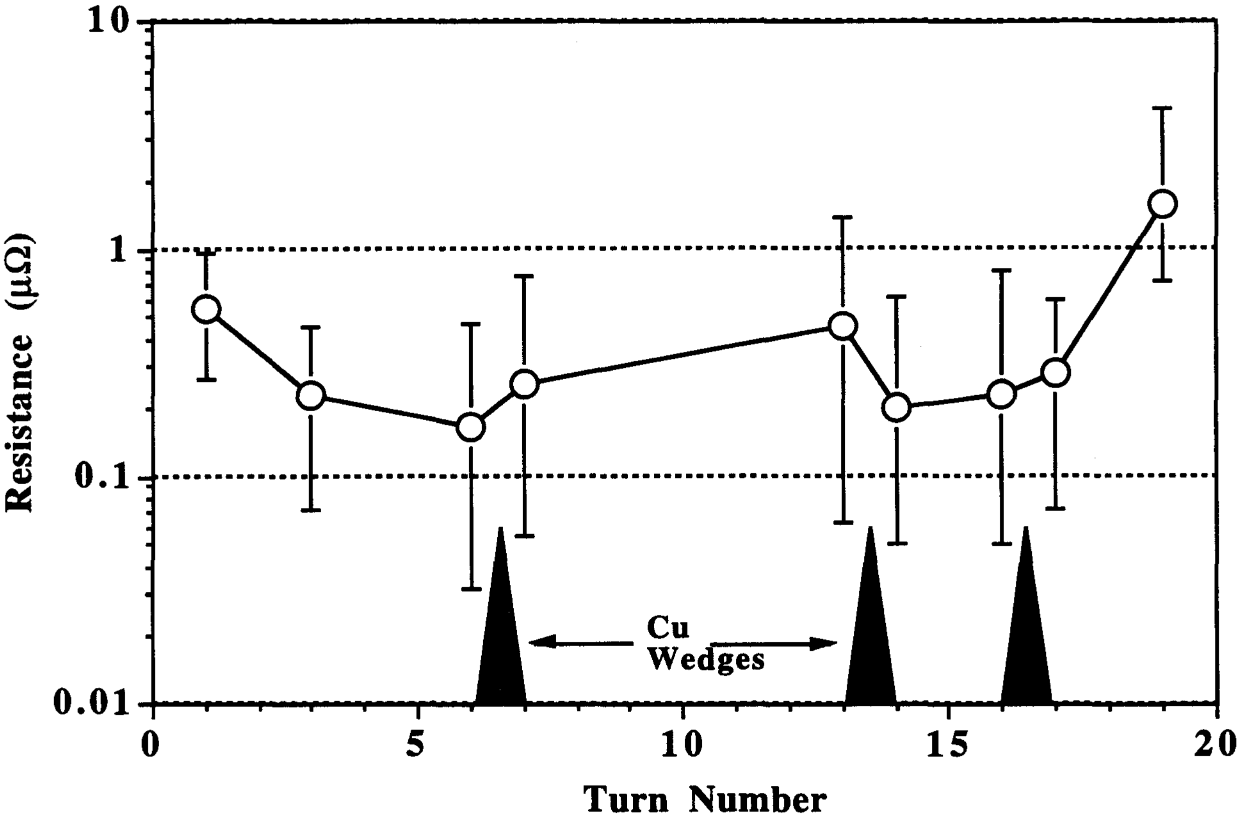

Figure 6. Distribution of average measured interstrand resistance at each coil turn for all test sections of magnet DCA312. The positions of the copper wedges are also depicted.

the fine structure of the interstrand resistance distribution shows variations of the average value from turn to turn which are greater than the measurement error. In this respect the most pronounced interstrand resistance variations can be seen at the wedge turns of the coil.

Also, for some unknown reason the wedge turn #6 (upper coil) has unusually high interstrand resistance. There has been speculation that the interstrand resistance distribution closely follows the prestress distribution in dipole magnets. However, this data does not simply correlate with prestress distribution calculations performed for SSC dipole magnets.[7]

In the case of DCA312 it is clear that the interstrand resistance tends to rise towards the midplane turn. As an illustration, the total (throughout all sixteen quadrants) average measured resistance vs. turn number of magnet DCA312 is shown in Figure 6. The maximum and minimum average measured resistances at each turn are indicated by the error bar symbols. One can see that the resistance tends to go down from the pole turn and then to go up towards the midplane, excepting some anomalies near the wedges. Thus, this data qualitatively correlates with the interstrand resistance distribution evaluated from DCA312 multipoles decay measurements.[8] The expected interstrand resistance distribution from analysis of multipoles decay measurements would be relatively large interstrand resistance at the pole and midplane and a minimum in the multiturn section of the coil.

III.6. Model for evaluation of interstrand losses and contact resistances

The first model for evaluating the interstrand resistance and interstrand eddy current losses in cables of superconducting accelerator magnets was proposed by G. Morgan.[9] Morgan's model neglects side-by-side contact of adjacent strands and assumes crossover resistance between any two strands of the cable to be identical. This model was developed for braid cables but it has also been used by some authors for evaluation of cable eddy currents in Rutherford type cables .[8]

The present results show that the interstrand resistances in a keystoned Rutherford cable under standard magnet prestress are not identical. Resistance between adjacent strands is considerably lower than the non-adjacent strand resistance. Also, resistances between the adjacent strands themselves as well as between non-adjacent strands vary and in many cases are far from identical. In a magnet coil under pressure the Rutherford cable is a very compact structure and can be considered as a specific network of superconducting wires located in a "solid" copper matrix with 2D or 3D anisotropy of effective electrical resistivity. The anisotropy of electrical resistivity accounts for different contact resistances between adjacent and non-adjacent strands. Such an approach represents an extension of the anisotropic continuum model for Rutherford type cables. The anisotropic continuum model was first proposed and developed by W. J. Carr, Jr. for describing electromagnetic coupling in multifilamentary superconductors.[10] The detailed description of the anisotropic continuum approach for evaluating the cable eddy current losses and interstrand resistances of SSC magnets is published elsewhere.[5] A brief discussion of the final equations for interstrand losses and evaluation of crossover resistances based on this model will be given here.

A sketch of a Rutherford cable showing the coordinate systems used in the following analysis is given in Figure 7. The total interstrand eddy current power loss per unit volume for a Rutherford type of cable is given by:

$$P/V = \frac{\dot{B}^2}{120} L^2 \sigma_\perp \left(\frac{a}{b}\right)^2 + \frac{\dot{B}^2}{3}\left(\frac{L}{4}\right)\sigma_\perp' + \frac{\dot{B}^2}{2R_{ed}}\left(\frac{L}{N}\right)\left(\frac{a}{b}\right) \qquad (5)$$

where $\dot{B}$ is the magnetic inductance ramp rate, **L** is the cable pitch length, **N** is the number of strands in the cable, **a** and **b** are the cable dimensions (Figure 7), $\sigma_\perp$ is the transverse conductivity in the **y** direction, $\sigma_\perp'$ is the transverse conductivity in the direction $\hat{a}_2$ and R_{ed} is the edge resistance. The first term of Equation (5) represents the eddy current losses due to crossover conductance in the cable. The second term gives the eddy current losses due to side-by-side conductance and the third term represents the losses due to the rollover contacts of strands at the cable edges. The dominant term is typically the loss between layers in the cable due to crossover conductance.

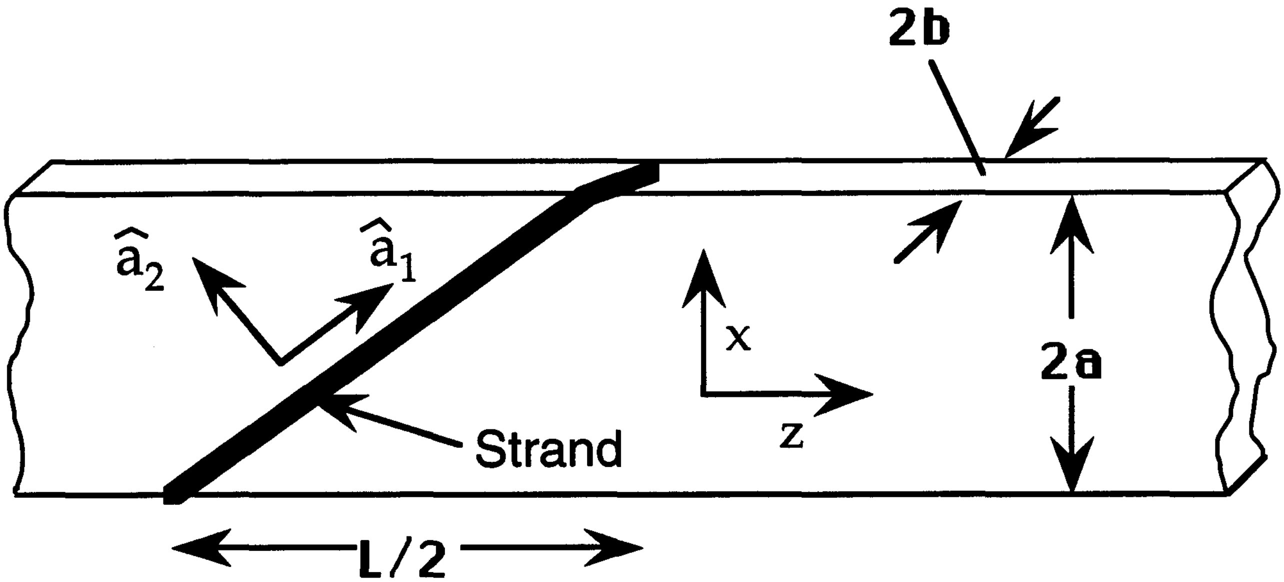

Figure 7. Strip of width 2a and thickness 2b representing a Rutherford cable of strands of twist pitch L. $\hat{a}_1$ and $\hat{a}_2$ are unit vectors parallel and perpendicular to the strand.

The crossover energy loss for the SSC cable for a bipolar cycle per unit length of the cable is given by:

$$Q/\dot{I} = \frac{1}{30}\left(\frac{B}{I}\right)^2 I_p N^2 L \,(2a)^2 \left\langle \frac{1}{R_c} \right\rangle \tag{6}$$

where $\dot{I}$ is the current ramp rate of the magnet, B is the magnetic induction, I is the cable current, I_p is the pick current in the cable, and R_c is the crossover resistance.

For the accelerator dipole magnets $(B/I)^2$ varies strongly with position of the turns in the magnet, since B is the component normal to the face of the conductor. $\langle 1/R_c \rangle$ is also not a constant. However, if $\langle 1/R_c \rangle$ is assumed to be constant and an average value of $(B/I)^2$ over the length of the cable is taken then for the SSC cable (a = 0.635 cm, b = 0.08 cm, L = 8.8 cm, N = 30) the crossover energy loss per unit magnet length becomes:

$$Q/\dot{I} = 9.6 \times 10^{-3}\, I_p \left\langle \frac{1}{R_c} \right\rangle \quad [\mathrm{J/A/s}] \tag{7}$$

where I is in Amps and R_c is in $\mu\Omega$.

Using the experimental value for eddy current losses of DCA312 obtained at Ip = 5000 A (multiplied by two for a bipolar cycle) Equation 7 gives a midplane value of $<R_c> = 5\ \mu\Omega$ which is a factor of 2 to 5 less than a typical midplane average crossover resistance evaluated for DCA312 from the interstrand resistance measurements. It is unrealistic to expect that any model results will fit exactly the test data for only four short sections (approximately 2% of the total magnet length) of such an anomalously behaving magnet as DCA312. The measurements of DCA312 have shown considerable variation of the interstrand resistance along the magnet axis and around the wedges. This can probably be attributed to either an initial non-uniformity in the cable and/or to non-uniformity in the coil preparation and assembly of this magnet. The detailed examination of the condition of the inner coil cable of this magnet after autopsy has confirmed severe deformation of cable strands at the minor and major edges and approximately 30% of the adjacent strands metallurgically bonded to each other. Also, the high ramp rate quenches of DCA312 (for instance at 200 A/s) were found to occur in the multiturn section of the coil far away from the midplane. This suggests that anomalously low interstrand resistance in these locations probably caused relatively large cable eddy currents in spite of the smaller $(B/I)^2$ there. Obviously, all technology based anomalies in the magnet behavior can not be considered or predicted by any analytical model. The fact that the interstrand resistance in the midplane of DCA312 is higher than for the multiturn sections of the inner coil can be seen on the resistance distribution curve shown in Figure 6.

The fit between the crossover resistance estimates based on the model and the test data for "normally" behaving magnets can be expected to be much better. Such a magnet is DSA328. Again considering the AC loss test data for DSA328 the model gives a midplane crossover resistance average of 92 $\mu\Omega$ and the interstrand resistance measurements on this magnet give a midplane value of 73 $\mu\Omega$. For DSA328 the interstrand resistance does not show any increase towards the midplane.

A very important result of the anisotropic continuum model for Rutherford cables is that the eddy current loss distribution will depend on the ratio between crossover, side-by-side, and rollover resistances. For instance if r_{co}/r_{adj} ($1/radj = 1/R_{ssl} + 2/R_{ed}$, where R_{ssl} and R_{ed} are side-by-side and rollover resistances respectively) is relatively small (< 10) almost the entire eddy current dissipation in the cable occurs due to crossover contacts. If $r_{co}/radj$ is relatively large (>100), then the dissipation between the adjacent strands could be significant.

IV. CONCLUSIONS

The following general conclusions can be drawn from the study of interstrand resistance in SSC magnets:

1). The resistances under standard magnet prestress at 4.2 K between adjacent strands are considerably lower than between non-adjacent strands. The non-adjacent strand resistances themselves vary from turn to turn, as well as in each particular turn along the magnet. This variation can exceed one order of magnitude. The resistances between adjacent strands vary considerably less than the non-adjacent resistances. The high ramp rate quench sites have lower interstrand resistances and a lower degree of interstrand resistance anisotropy (smaller ratio r_{co}/r_{adj}) than the rest of the coil.

2). The interstrand resistance distribution in the magnet coil appears to be an unique function of cable and coil technology and/or magnet assembly procedure. The interstrand resistance shows considerable irregularity around the wedges. The interstrand resistance decreases from the pole turn and remains constant or increases toward the midplane. The interstrand resistance distribution affects mutipoles decay and must be controlled strictly in order to build magnets with predictable multipole characteristics.

3). The eddy current loss distribution in each particular turn of the coil will depend on the interplay between crossover, side-by-side, and rollover resistances. If crossover conductance dominates, then the eddy current dissipation in the cable occurs mainly between layers of the cable. If side-by-side and rollover conductance is relatively high, then the eddy current loss within the layers and at the edges of the cable will be significant.

V. ACKNOWLEDGMENTS

The authors wish to thank Dr. C. Haddock and Dr. J. Seuntjens for useful discussion and T. Jarrett , S. Graham, P. Cline, J. Qin, and J. Madison for helping with sample preparations and measurements.

VI. REFERENCES

1). M. Wake, Ramp rate behavior of SSC magnets, MSD Technical Note # MD-MKA-0-93-007, SSCL, June 23, 1993.

2). C. Swenson, Magnet Autopsy Test Plan: DCA312, WMSD, Round Rock, TX, March 1993.

3). V. T. Kovachev, M. J. Neal, J. M. Seuntjens, J. Qin, P. G. Cline, C. Swenson, and D. W. Capone II, Interstrand Resistance of Selected Sections of DSA312, SSCL-651, November 1993.

4). V. T. Kovachev, M. J. Neal, J. M. Seuntjens, J. Madison, S. Graham, P. G. Cline, M. Wake, and D. W. Capone II, Interstrand Resistance of DSA328 Coil, SSCL-637, August 1993.

5) M.J. Neal and V. T. Kovachev , Models for Evaluating *In Situ* Interstrand Resistance Measurements (in press).

6) W.J. Carr, Jr. and V. T. Kovachev , Interstrand Eddy Current Losses in SSC magnets (in press)

7). J. Turner, Mechanical Analysis of the W6733H Cross-Section, MSD Technical Note #MD-TA-143, SSCL, July 1990.

8). T. Ogitsu et. al., Influence of eddy currents on magnetic field harmonics, Proc. ICFA Workshop on AC Superconductivity, 23, KEK, Tsukuba, Japan, 1992

9). G. H. Morgan, Eddy currents in flat metal-filled superconducting braids, J. Appl. Phys., 44, 3319 (1973)

10 W.J. Carr, Jr. , AC Loss and macroscopic theory of superconductors, Gordon & Breach, N.Y., 1983